https://doi.org/10.5194/acp-2020-1276
Preprint. Discussion started: 28 December 2020

Atmospheric Chemistry and Physics Discussions

Impacts of Secondary Ice Production on Arctic Mixed-Phase Clouds based on ARM Observations and CESM2

Xi Zhao[1], Xiaohong Liu[1], Vaughan T. J. Phillips[2], and Sachin Patade[2]

[1]Department of Atmospheric Sciences, Texas A&M University, College Station, Texas, 77840, USA

[2]Department of Physical Geography and Ecosystem Science, Lund University, Lund, Sweden

Correspondence to: Xiaohong Liu (xiaohong.liu@tamu.edu)

Abstract. For decades, measured ice crystal number concentrations have been found to be orders of magnitude higher than measured ice nucleating particles in moderately cold clouds. This observed discrepancy reveals the existence of secondary ice production (SIP) in addition to the primary ice nucleation. However, the importance of SIP relative to primary ice nucleation remains highly unclear. Furthermore, most weather and climate models do not represent well the SIP processes, leading to large biases in simulated cloud properties.

This study demonstrates a first attempt to represent different SIP mechanisms (frozen raindrop shattering, ice-ice collisional break-up, and rime splintering) in a global climate model (GCM). The model is run in the single column mode to facilitate comparisons with the Department of Energy (DOE)'s Atmospheric Radiation Measurement (ARM) Mixed-Phase Arctic Cloud Experiment (M-PACE) observations.

https://doi.org/10.5194/acp-2020-1276
Preprint. Discussion started: 28 December 2020

Atmospheric Chemistry and Physics
Discussions

We show the SIP importance in the four types of clouds during M-PACE (i.e., multilayer, and single-layer stratus, transition and front clouds), with the maximum enhancement in ice crystal number concentration by up to 4 orders of magnitude in the moderately-cold clouds. We reveal that SIP is the dominant source of ice crystals near the cloud base for the long-lived Arctic single-layer mixed-phase clouds. The model with SIP improves the occurrence and phase partitioning of the mixed-phase clouds, reverses the vertical distribution pattern of ice number concentration, and provides a better agreement with observations. The findings of this study highlight the importance of considering the SIP in GCMs.

https://doi.org/10.5194/acp-2020-1276
Preprint. Discussion started: 28 December 2020

1 Introduction

Clouds play a critical role in the surface energy budget of the Arctic, thereby affecting the Arctic sea ice and regional climate (Kay et al., 2009; Bennartz et al., 2013). Clouds frequently occur in the Arctic (Beaufort Sea) with an observed annual mean cloud occurrence of 85%, a maximum of 97% in September, and a minimum of 63% in February (Intrieri et al., 2002). Along with the occurrence frequency, the phase partitioning between liquid and ice in mixed-phase clouds, i.e., the clouds where liquid and ice coexist at subfreezing temperatures, is also important, since even a small amount of liquid content in clouds can substantially change the radiative properties of the cloud (Shupe et al., 2004; Cesana and Chepfer, 2013). Shupe et al. (2006) showed that over the Beaufort Sea, 59% of observed clouds were mixed-phase, while another study indicated 90% over the western Arctic Basin (Pinto, 1998).

Mixed-phase clouds are microphysically unstable. Even a small amount of cloud ice can glaciate the mixed-phase clouds in a few hours via the Wegener–Bergeron–Findeisen (WBF) mechanism (Morrison et al., 2012). Mixed-phase clouds in the Arctic are long-lived and characterized by a structure with liquid water at the cloud top and ice water underneath. Interaction and feedback between multiple processes, including longwave radiative cooling, turbulent entrainment, and condensation of liquid water, provide sufficient moistening and cooling at the cloud top. This sustains enough formation of liquid

https://doi.org/10.5194/acp-2020-1276
Preprint. Discussion started: 28 December 2020

mass against the depletion by the WBF process. In order to support the self-maintenance of liquid water, low concentrations of small ice particles must be present near the cloud base (Shupe et al., 2006; Korolev and Field, 2008). In this way, they are efficient in sedimentation (Jiang et al., 2000) but less active in the WBF and vapor deposition processes. Previous studies indicated that 90% of Arctic mixed-phase cloud temperature was between -25°C and -5°C from an annual mean perspective (Shupe et al., 2006), indicating that ice exists in moderately supercooled clouds. However, the mechanisms contributing to ice formation in these clouds are still unclear (Shupe et al., 2006; Morrison et al., 2012). One objective of this study is to better understand the ice formation processes in the mixed-phase Arctic clouds.

Previous studies have shown the important role of SIP in the Arctic cloud from observations (Schwarzenboeck et al., 2009) and small-scale model simulation. Using a large-eddy simulation (LES) model and a Lagrangian parcel model, Sotiropoulou et al. (2020a) found that a combination of ice-ice collisional fragmentation and rime splintering provides a better agreement of the simulated ice crystal number concentration (ICNC) with observations in the summer Arctic stratocumulus. They found a low sensitivity of SIP to prescribed cloud condensation nuclei (CCN) and ice nucleating particles (INPs). In addition, their study highlighted the importance of considering ice-ice collisional fragmentation in large-scale models. Fu et al. (2019) simulated an autumnal Arctic single-layer boundary-layer mixed-phase cloud using the Weather Research and Forecasting

https://doi.org/10.5194/acp-2020-1276
Preprint. Discussion started: 28 December 2020

(WRF) model and showed that the model without considering SIP needs an increase of INPs by two orders of magnitude to match the observed ICNCs. In comparison, the model that only considers the SIP through droplet shattering needs an INP increase of 50 times to match the observed ICNCs. Sotiropoulou et al. (2020b) simulated a summer boundary layer coastal cloud in West Antarctica using the WRF model and found that the model with collisional break-up between ice-phase particles can reproduce the observed ICNCs, which could not be explained by the rime splintering or primary ice nucleation. Sullivan et al. (2017) used a parcel model with rime splintering and graupel-graupel collisional break-up and found that these two SIP processes can enhance the ICNCs by four orders of magnitude. Sullivan et al. (2018a) showed that among the different SIP mechanisms, only ice–ice collisional fragmentation contributes to a meaningful ice enhancement (larger than 0.002 L^{-1}) in a parcel model simulation. They also found that a modest updraft and a warm cloud base significantly affect the onset of rime splintering and droplet shattering. Other studies have shown the impact of SIP on ICNCs in a cold frontal rain band over the UK (Sullivan et al., 2018b), on surface precipitation of a tropical thunderstorm (Connolly et al., 2006) and the summertime cyclones (Dearden et al., 2016).

Previous studies have used multi-scale models, including small-scale models such as parcel models, LES models as well as regional models, to investigate the impacts of SIP on cloud properties. However, there is still a lack of a large-scale perspective based on a global climate model. Moreover, the mechanisms contributing to the ice production in

Atmospheric Chemistry and Physics Discussions
Open Access
EGU

Arctic mixed-phase clouds at moderately cold temperatures are still unknown. In this study, for the first time, we have implemented multiple SIP mechanisms (i.e., raindrop shattering, ice-ice collisional break-up, and rime splintering) in a global climate model (GCM). We test the model performance by running the model in the single column mode (SCM) and compare the SCM simulations of Arctic clouds with observations. The objectives of this study are to examine the impact of SIP on different types of Arctic clouds and, ultimately to improve the model capability of representing ice processes.

This paper is organized as follows. In section 2, we describe the GCM, associated parameterizations, and three SIP mechanisms represented in the model. In section 3, we present the model experiments and observation data used for model evaluation. The model results are presented in section 4. The main conclusions of this study and future work are summarized in section 5 and 6.

2 Model and Parameterizations

2.1 Model description

The Community Atmosphere Model version 6 (CAM6) used in the current study is the atmosphere component of the Community Earth System Model version 2 (CESM2). It includes multiple physical parameterizations that are related to ice formation and evolution. Cloud microphysics is described by a double-moment microphysical scheme based on

https://doi.org/10.5194/acp-2020-1276
Preprint. Discussion started: 28 December 2020

Gettelman and Morrison, 2015. The scheme considers homogeneous freezing of cloud droplets (with temperatures below –40 °C), heterogeneous freezing of cloud droplets, the Wegener–Bergeron–Findeisen process, accretion of cloud droplets by snow, and the riming splintering. Secondary ice production from rime splintering is parameterized based on Cotton et al. (1986). The condensation process is also known as cloud macrophysics, which is governed by the Cloud Layers Unified by Binormals (CLUBB) scheme, assuming that all the condensate is in the liquid phase (Golaz et al., 2002; Larson et al., 2002). Furthermore, CLUBB also treats boundary layer turbulence and shallow convection. In the mixed-phase clouds, heterogeneous ice nucleation is represented by the classical nucleation theory (CNT), which relates ice nucleation rate to mineral dust and black carbon aerosols (Wang et al., 2014). In cirrus clouds, where temperatures are below –37 °C, heterogeneous immersion freezing on dust can compete with homogeneous freezing of sulfate (Liu and Penner, 2005). The aerosol species involved in ice nucleation processes are represented by the four-mode version of the Modal Aerosol Module (MAM4) (Liu et al., 2012; Liu et al., 2016).

In this study, we have conducted the CAM6 simulations in SCAM. SCAM is a one-column, time-dependent model configuration of CAM6 that provides an efficient way to understand the behavior of model physical parameterizations without the influence of nonlinear feedbacks from the large-scale circulation. In this way, the biases of the modeled clouds can be exclusively identified from model evaluation against observations.

https://doi.org/10.5194/acp-2020-1276
Preprint. Discussion started: 28 December 2020

Atmospheric Chemistry and Physics Discussions

2.2 Implementation of secondary ice production in CESM2

In addition to existing SIP mechanisms in CAM6, we implemented two mechanisms of SIP, including ice-ice fragmentation and droplet shattering (Phillips et al., 2017a, 2018) that are based on theoretical and measurement research.

a. An emulated bin framework

Ideally, bin microphysics is the most suitable model setup for representation of SIP mechanisms in a cloud model. However, running a GCM model with a bin microphysics is computationally too expensive under current computational resources. To solve this problem, we developed an emulated bin framework for the existing bulk microphysical scheme to facilitate the coagulation of ice hydrometeors and rain. First, we selected the bin bounds for each hydrometeor, including cloud ice, snow, and rain. A logarithmically equidistant size grid is adopted, that is,

$$D_{k+1} = CD_k, \tag{1}$$

where $C = \sqrt[4]{2}$

The bin diameter ranges from 0.1 to 6 mm for raindrops and 0.1 to 50 mm for snow and cloud ice particles. Based on the assumption of the particle size distribution, the number concentration and mass mixing ratio of all hydrometeor types was calculated in each temporary bin at each time step and grid point. The estimated particles size distribution from the emulated bin framework serves as inputs for the SIP schemes. The

https://doi.org/10.5194/acp-2020-1276
Preprint. Discussion started: 28 December 2020

Atmospheric Chemistry and Physics Discussions

SIP schemes were applied to each permutation of the bin during coagulation of ice, snow, and rain to calculate the secondary ice fragments. Finally, we summed up the fragment from SIP over all pairs of bins.

b. Ice-ice fragmentation

Phillips et al. (2017a, b) developed a scheme for SIP during an ice-ice collision based on the principle of energy conservation. This scheme relates the fragment numbers to particle initial kinetic energy and ice particle habits (i.e., ice morphology), which can be explained in terms of environmental temperature, particle size, and riming intensity of ice particles (Fig. 1). The production of new ice particles per collision is calculated as:

$$\mathcal{N} = \alpha A \left[1 - e^{-\left(\frac{Ck_0}{\alpha A}\right)^{\gamma}}\right] \tag{2}$$

in which α is the surface area of ice particle, i.e., the equivalent spherical area in a unit of m^2, $\alpha = \pi D^2$; A is the number density of breakable asperities of ice particles, which is related to riming intensity and ice particle size; C is the asperity-fragility coefficient, prescribed to be 10815 for dendrites and 24780 for spatial planar; γ is a parameter related to riming intensity (rim), $\gamma = 0.5 - (0.25 \times rim)$; k_0 is the initial kinetic energy, which is given as:

https://doi.org/10.5194/acp-2020-1276
Preprint. Discussion started: 28 December 2020

Atmospheric Chemistry and Physics Discussions

$$k_0 = \frac{1}{2}\frac{m_1 m_2}{m_1+m_2}(v_1 - v_2)^2 \quad (3)$$

in which m_1 and m_2 are the particle masses of two colliding particles, and v_1 and v_2 are the terminal velocities of the two colliding particles.

In this method, three types of collision are identified based on the type of collision particles: (1) cloud ice/snow collide with hail/graupel; (2) cloud ice/snow collide with cloud ice/snow; (3) hail/graupel collide with hail/graupel (not included currently, since CESM2-CAM6 does not treat graupel currently);. For each collision type, different values of parameters α, A, C, and γ in Eq. (1) are yielded based on the measured relationship between fragment number and collisional kinetic energy (Phillips et al., 2017a).

Under the emulated bin framework, the new fragment production rate for each permutation of a bin is written as:

$$N_{iic} = \mathcal{N}\ E_c \delta N_1 \delta N_2 \pi (r_1 + r_2)^2 |v_1 - v_2| \quad (4)$$

in which E_c is the accretion efficiency, and δN_1 and δN_2 are the particle number concentrations in the two bins with particle sizes of r_1 and r_2, respectively.

The ice production rate for cloud ice mixing ratio is:

$$P_{iic} = N_{iic} \delta m_{ice} \quad (5)$$

in which δm_{ice} is mass for single ice particle, prescribed as 2.09×10^{-15} kg.

https://doi.org/10.5194/acp-2020-1276
Preprint. Discussion started: 28 December 2020

c. Droplet shattering during rain freezing

Phillips et al. (2018) proposed a numerical formulation for ice multiplication during the raindrop freezing. They suggested two modes of droplet break-up during the rain freezing based on the relative weight of raindrop and ice particle (Fig. 2).

In mode 1, the freezing of rain is triggered by a collision with less massive ice crystals or with INPs. By fitting a formulation to the laboratory dataset, Phillips et al. (2018) derived an empirical formulation for the number of ice fragments per frozen raindrop as a function of drop diameter and temperature. A Lorentzian distribution as a function of temperature was adopted to represent the number of ice fragments per frozen raindrop. There are two types of raindrop fragmentation: shattering to form broken halves or a third of similar sizes known as 'large' fragments and 'tiny' splinters with less than 10% of the original drop mass. The total (large+tiny) and large ice fragments per frozen raindrop emitted in the mode 1 of droplet shattering are given in Eqs. (6) and (7), respectively:

$$\mathcal{N}_T = F(D)\Omega(T)\left[\frac{\zeta\eta^2}{(T-T_0)^2+\eta^2} + \beta T\right] \tag{6}$$

$$\mathcal{N}_B = min\left\{F(D)\Omega(T)\left[\frac{\zeta_B\eta_B^2}{(T-T_{B0})^2+\eta_B^2}\right], \mathcal{N}_T\right\} \tag{7}$$

where the parameters $\zeta, \eta, \beta, T_0, T_{B0}$ are derived by fitting the formulations to a collection of laboratory data. Further details about on empirical formulation can be found in Phillips et al. (2018). $F(D)$ and $\Omega(T)$ are the interpolating functions for the onset of fragmentation

https://doi.org/10.5194/acp-2020-1276
Preprint. Discussion started: 28 December 2020

and T is the temperature in K. The mass of a large fragment is $m_B = \chi_B m_{rain}$, in which $\chi_B = 0.4$, and the mass of a small fragment is $m_S = \frac{\pi \rho_i}{6} D^3$, in which $\rho_i = 920\ kg\ m^{-3}$.

The observational data used for the formulation of raindrop freezing by mode 1 was limited to drop diameter of 1.6 mm and a temperature range between –4 °C to –25 °C. Phillips et al. (2018) linearly extrapolated their algorithm for mode 1 for larger particles and other temperatures in the mixed-phase cloud regime. As shown in the Fig. 2a, b, mode 1 of the droplet shattering is most effective near -15°C.

In mode 2, a theoretical approach is adopted which is based in the assumption that the number of fragments generated when a drop collides with a more massive ice particle is controlled by the initial kinetic energy and surface energy (Fig. 2c). The number of fragments generated per frozen drop in mode 2 is given as:

$$\mathcal{N}_{fr2} = 3\Phi(T) \times [1 - f(T)] \times \max(DE - DE_c), \quad (8)$$

where DE is the dimensionless energy and is expresses as:

$$DE = \frac{k_0}{S_e}, \quad (9)$$

where k_0 is the initial kinetic energy which is given in Eq. (3), S_e is the surface energy, expressed as $S_e = \gamma_{liq} \pi D^2$, γ_{liq} is the surface tension of liquid water which is 0.073 J m^{-2}. DE_c in Eq. (8) is set to be 0.2. $f(T)$ is the frozen fraction (Phillips et al., 2018), and is given as:

https://doi.org/10.5194/acp-2020-1276
Preprint. Discussion started: 28 December 2020

$$f(T) = \frac{-C_w T}{L_f}. \quad (10)$$

where C_w is the specific heat capacity of liquid water (4200 J kg^{-1} K^{-1}) and L_f is the specific latent heat of freezing (3.3×10^5 J kg^{-1}), $\Phi(T) = 0.5$ at –1°C and $\Phi(T) = min\,[4f(T), 1]$.

d. Rime splintering

The CESM2-CAM6 microphysics already includes the SIP associated with riming splintering, which is also known as Hallet-Mossop (HM) process. In this process, secondary ice particles are generated during the accretion of cloud droplets by snow, and a part of rimed mass is converted to cloud ice. The ice number production rate is based on the parameterization of Cotton et al. (1986) and is given as:

$$N_{HM} = C_{sip\_HM} \times p_{sacws} \quad (11)$$

where p_{sacws} is the riming rate of cloud droplets by snow, and the conversion coefficient C_{sip_HM} depends on temperature T_c in °C:

$$C_{sip\_HM} = \frac{3.5\times10^8\times(-3-T)}{2}, \text{ when } -5 < T_c < -3, \text{ and} \quad (12)$$

$$C_{sip\_HM} = \frac{3.5\times10^8\times(T-(-8))}{3}, \text{ when } -8 < T_c < -5 \quad (13)$$

The riming splintering rate as a function of p_{sacws} and temperature is shown in Fig. 3.

https://doi.org/10.5194/acp-2020-1276
Preprint. Discussion started: 28 December 2020

3 Case Description, Observations, and Model Experiments

3.1 M-PACE case

In this study, we focus on the Arctic mixed-phase clouds observed during the Department of Energy (DOE)'s Atmospheric Radiation Measurement (ARM) Mixed-Phase Arctic Cloud Experiment (M-PACE). The M-PACE campaign was conducted over the North Slope of Alaska (NSA) during the autumn period from 27 September to 22 October 2004.

Various types of clouds were observed during M-PACE campaign, including multilayer stratus, thin boundary layer mixed-phase stratus clouds, cirrus, and altostratus clouds associated with the frontal system (Verlinde et al., 2007; Liu et al., 2007; Xie et al., 2008; Liu et al., 2011). Single-layer mixed-phase clouds were formed under moderately supercooled conditions with the cloud temperature at around –10 °C (Verlinde et al., 2007; McFarquhar et al., 2007), providing a favorable condition for studying the influence of SIP on cloud evolution (Field et al., 2016).

The synoptic-scale systems regulated the properties of clouds observed during the M-PACE campaign. Hence, Verlinde et al. (2007) divided the M-PACE period into three synoptic regimes and two transition periods based on the synoptic weather conditions. The first synoptic regime began on 24 September and lasted until 1 October, 2004, when a well-developed trough dominated aloft with several low-pressure systems that influenced the

https://doi.org/10.5194/acp-2020-1276
Preprint. Discussion started: 28 December 2020

Atmospheric Chemistry and Physics Discussions
Open Access
EGU

surface. Followed by the first transition period between 2 and 3 October, the second synoptic regime occurred between 4 and 14 October (Fig. 4), which was controlled by a pronounced high-pressure system. The second transition period was from 15-17 October. By 18 October, a fast-developing strong frontal system controlled the cloud formation over the NSA in the third synoptic regime (Fig. 4). During M-PACE, the surface flux of water vapor, sensible heat, and latent heat played a different role in cloud formation. For example, clouds formed in response to a strong surface forcing during the second regime, while clouds formed under a relatively weak surface forcing during the third regime. In this study, we evaluate modeled cloud properties with M-PACE observations in the second and third synoptic regimes focusing on the boundary layer mixed-phase stratus during 9-12 October in the second regime.

3.2 Observation data

The observed cloud occurrence data at Barrow (located at: 71.3° N 156.6° W) are from the ARM Climate Modeling Best Estimate product (Xie et al., 2010). The liquid water path (LWP) was measured using the ARM Climate Facility operational Microwave Radiometer with different retrieved algorithms (Wang 2007; Turner et al., 2007). The ice water path (IWP) was using the ARM Millimeter Wavelength Cloud Radar and Micropulse Lidar. Note that measured IWC and IWP cannot distinguish cloud ice from the snow. The

https://doi.org/10.5194/acp-2020-1276
Preprint. Discussion started: 28 December 2020

simulated IWP and ice water content (IWC) therefore include the snow component which is consistent with observations used in this study.

During M-PACE campaign, the ICNC was measured during the single-layer mixed-phase stratus period. The data includes 53 profiles measured during four flights over Barrow and Oliktok Point (located at: 70.5° N 149.9° W) using the instrumented aircraft by the University of North Dakota Citation. By combining measurements from different probes, McFarquhar et al. (2007) provided cloud particle size distributions over a continuous size range. The forward scattering spectrometer probe (FSSP) measured particle number concentrations with particle diameters between 3 to 53 μm, while the one-dimensional cloud probe (1DC) counted cloud particles ranging from 20 to 620 μm. The two-dimensional cloud probe (2DC) covered particle sizes from 30 to 960 μm, while the high-volume precipitation sampler (HVPS) sampled particles from 0.4 to 40 mm. The data were collected every 10 seconds but were averaged to 30 s^{-1} to ensure adequate statistical sampling. The cloud phase was identified by detecting the presence of supercooled droplets by the Rosemount Icing Detector (RICE). In mixed-phase clouds, any particles larger than 125 μm are identified as ice particles, and cloud particles smaller than 53 μm are counted as liquid-phase particles. Particles with a diameter ranging from 53 to 125 μm are counted as a liquid when there is drizzle, and as ice, if there is no drizzle. A more detailed description of the particle phase identification algorithm can be found in McFarquhar et al. (2007). When comparing the

https://doi.org/10.5194/acp-2020-1276
Preprint. Discussion started: 28 December 2020

simulated ICNC with the observations, only ice particles larger than 53 μm were considered, as the observations were limited to ice particles larger than 53 μm.

3.3 Model set up and description of model experiments

In this study, we run SCAM with 32 vertical layers from the surface up to 3 hPa. The model is driven by the large-scale forcing data every 3 hours, which were developed based on Xie et al. (2006). The simulation period is from 5 to 22 October 2004 and covers the second and third synoptic regimes and the transition period between them.

A detailed description of model experiments along with SIP mechanisms in these experiments is provided in Table 1. The control model experiment (CTL) uses the default CAM6 model that does not include SIPs due to the ice-ice collision break-up and rain freezing fragmentation. The impacts of SIP mechanisms, including ice-ice collision break-up and rain freezing fragmentation processes based on Phillips et al. (2017a, 2018) are addressed in SIP_PHIL experiment. To examine the impact of rime splintering in the CTL experiment, we conducted CTL_no_HM experiment that is similar to CTL but without HM process.

https://doi.org/10.5194/acp-2020-1276
Preprint. Discussion started: 28 December 2020

4 Results

4.1 SIP impacts on different types of clouds during M-PACE

Figure 4 shows the temporal evolution of LWP, IWP, and cloud fractions from two model simulations (CTL and SIP_PHIL) and their comparison to observations. The model simulations cover the second and third synoptic regime as well as the transition period between them. Two different types of clouds were formed in response to the strong surface forcing during the second synoptic regime from 4 to 14 October. As shown in Fig. 4c, multilayer stratus occurred from 5 to 8 October, and the clouds extended up to 500 hPa from 950 hPa. Between 9 and 14 October, single-layer boundary layer mixed-phase stratus occurred between 800-950 hPa. Because of the dramatic change in cloud types in the second regime, we further separate the second regime into two time periods. Then, we select typical days in the four time periods for our analysis in this study, as shown in Fig. 4. The period from 6 to 8 October is selected as the "multilayer stratus" period. The period between 9 to 14 October is selected as the "single-layer stratus" period, followed by the transition period marked on 16 October. The period between 18 and 20 October is selected to represent the "frontal cloud" type during the third regime.

Figure 4 shows that the simulated IWP is systematically underestimated during M-PACE in the CTL experiment. The maximum value of IWP in CTL is smaller than 50 g m^{-2} during M-PACE, but up to 500 g m^{-2} in measurements. The SIP_PHIL experiment shows

https://doi.org/10.5194/acp-2020-1276
Preprint. Discussion started: 28 December 2020

Atmospheric Chemistry and Physics Discussions

decreased LWP and increased IWP compared with CTL, reaching a better agreement with the measurements. For example, IWP increases from 50 g m^{-2} in CTL to 425 g m^{-2} in SIP_PHIL on 20 October, compared with 300 ~ 475 g m^{-2} from different measurements (Fig. 4). The simulated LWP is overestimated during the "multilayer stratus" and "frontal cloud" periods in CTL, especially on 20 October. The SIP_PHIL experiment decreases the LWP from 425 g m^{-2} in CTL to 70 g m^{-2} on 20 October (Fig. 4a).

4.1.1 Multilayer stratus

The CTL and SIP_PHIL experiments show that during the multilayer stratus period, the cloud top is located about 5 km at a temperature of –20 °C (Fig. 5). These cloud properties are consistent with the observations (Verlinde et al., 2007) that show a minimum observed cloud temperature of –17°C (Fig. 4). However, we notice a significant overestimation of cloud amount at 6–8 km on 7 October by the model simulations in Fig. 5, as compared to the observations in Fig. 4c.

During the multilayer stratus period, IWC is increased in the SIP_PHIL simulation compared to CTL, while liquid water content (LWC) is decreased. The mean vertical profiles of simulated IWC and LWC in the multilayer stratus period are shown in Fig. 6. The simulated values of LWC and IWC are lower than observations, particularly for IWC. LWC decreases from 130 mg m^{-3} in CTL to 80 mg m^{-3} in SIP_PHIL below 1 km. IWC increases

https://doi.org/10.5194/acp-2020-1276
Preprint. Discussion started: 28 December 2020

from 3 mg m^{-3} in CTL to 5 mg m^{-3} in SIP_PHIL. The time-averaged IWP increases from 11.2 g m^{-2} in CTL to 17.1 g m^{-2} in SIP_PHIL but is still lower than the observed value of 55.6 g m^{-2} (Table. 2). After considering the SIP in the model, for the multilayer stratus period, ICNC is increased by 1 L^{-1} (Fig. 5) at an altitude of 1 to 4 km. Observations of ICNC are not available during this period.

4.1.2 Boundary-layer mixed-phase stratus

Between 9 and 14 October, a persistent boundary-layer mixed-phase stratus occurred between 800-950 hPa, with the cloud top temperature at around –15 °C (Fig. 4c). This single-layer stratus was separated from the surface based on the measurement (Fig. 4c). However, modeled clouds extend to the surface in CTL (Fig. 5). This bias is alleviated in SIP_PHIL, and the clouds decouple from the surface during 8–12 October (Fig. 5). Previous studies also found that this bias partially results from the overestimation of low-level moisture in the large-scale forcing data (Zhang et al., 2019, 2020).

Observed cloud liquid is located above the cloud ice during this period, with the LWC peak ~0.5 km above the IWC peak. Observed vertical profile of LWC shows a maximum of 300 mg m^{-3} (ranging from 210 to 500 mg m^{-3}) at ~1.25 km, while observed IWC is peaked at 0.75 km (Fig. 6). This characteristic is clearly captured by the SIP_PHIL experiment, with the peaks of LWC and IWC located at 0.75 and 0.5 km, respectively (Fig. 6). A better relative

https://doi.org/10.5194/acp-2020-1276
Preprint. Discussion started: 28 December 2020

position of cloud liquid and ice in SIP_PHIL indicates a better simulation of interactions between cloud physics and dynamics. This distinct feature also contributes to the longevity of mixed-phase clouds in the Arctic, as discussed in Section 1.

In SIP_PHIL, the maximum IWC value is four times larger than that in CTL (2 versus 0.5 mg m^{-3}); accordingly, mean IWP increases from 0.9 in CTL to 2.5 g m^{-2} in SIP_PHIL (Table 2). Meanwhile, ICNC in SIP_PHIL is higher than that in CTL, and the maximum ICNC goes up by 5 L^{-1} at 0.5 km on 11 October (Fig. 5). Thus, SIP adds an extra source of ice crystals to the boundary-layer mixed-phase stratus clouds.

4.1.3 Transition period

During the transition period, several distinct liquid layers are interrupted by the ice enriched layers in the observation. Due to the coarse vertical resolution, the model may not be able to capture this vertical variation accurately. Considerable variation was noticed in the observed IWC with a maximum IWC of 0. 8–1.8 mg m^{-3}. The CTL experiment substantially underestimates IWC, as it produces IWC less than 0.1 mg m^{-3} (Fig. 7). The maximum IWC in SIP_PHIL is 1.15 mg m^{-3}, providing a better agreement with the observation. The temporally-averaged IWP from SIP_PHIL is 10^4 times larger than that from CTL, with values of 0.0001, 3.6, and 5.6 g m^{-2} in CTL, SIP_PHIL, and observation, respectively (Table 2). The vertically-integrated ICNC is 7.66 and 4.57×10^5 L^{-1} in CTL and SIP_PHIL,

https://doi.org/10.5194/acp-2020-1276
Preprint. Discussion started: 28 December 2020

Atmospheric Chemistry and Physics Discussions

respectively (Table 2). Considering SIP in the model increases column integrated ICNC by five orders of magnitude during the transition period.

4.1.4 Frontal clouds

During the frontal cloud period, the SIP_PHIL experiment shows highest absolute increase in IWC and ICNC compared to the other periods. Stratocumulus and altostratus clouds (Verlinde et al., 2007) associated with the frontal system extend from the surface up to 8 km in the measurements and simulations (Fig. 5). The peak of modeled IWC is located at 2.5 km, with values of 2 and 8 mg m^{-3} in CTL and SIP_PHIL respectively (Fig. 7), much lower than the observation (ranging from 8 to 40 mg m^{-3}). IWP is 96, 10.4 and 26.1 g m^{-2} in the observation, CTL, and SIP_PHIL, respectively (Table 2). ICNC is increased by up to 7 L^{-1} between 2 to 4 km on 20 October from CTL to SIP_PHIL (Fig. 5). IWP and ICNC in SIP_PHIL are about two times of those in CTL.

4.1.5 SIP versus primary ice production in different types of clouds

The relative importance of primary and secondary ice production is shown as pie charts in Fig. 8, to identify the dominant ice production mechanism in different types of Arctic clouds. The primary ice production (i.e., ice nucleation) is more important in the clouds with colder cloud tops, such as multilayer stratus and frontal clouds with cloud top temperatures colder than –25 °C and –40 °C, respectively. The primary ice production

https://doi.org/10.5194/acp-2020-1276
Preprint. Discussion started: 28 December 2020

contributes 37% and 69% to the total ice production during the multilayer stratus and frontal cloud periods, respectively. Primary ice production is more efficient in deep clouds due to the inverse relationship between the ice nucleation rate and temperature. SIP is more important than primary ice production in the boundary-layer stratus and in clouds during the transition period when cloud top temperatures were at -15 °C. The fragmentation of freezing raindrops contributes the most (up to 80%) to the ice production in the single-layer boundary-layer stratus. The break-up from ice-ice collisions contributes 22% to the total ice production in the frontal clouds, while the rime splintering contributes 22% to the multilayer stratus. These two SIP mechanisms account for a small fraction of the ice production in the boundary-layer stratus.

Next, we will focus on the SIP impacts on the boundary-layer mixed-phase stratus related to the phase partitioning (section 4.2) and ICNC (section 4.3).

4.2 SIP impact on occurrence and phase partitioning of the mixed-phase clouds

Figure 9 shows the liquid fraction (defined as LWC/(LWC+IWC)) as a function of normalized height in the single-layer boundary-layer mixed-phase stratus. The normalized height Z_n is 0 at cloud base and 1 at cloud top. IWC from the model includes all the ice hydrometeors to compare it with observations. Measurements showed in Fig. 9a reveal two features of the single-layer boundary-layer clouds: (1) mixed-phase is dominant in clouds, and (2) the liquid fraction increases with cloud altitude. The liquid fraction is between 0.05 and 0.95 in most portions of the clouds, indicating a mixed-phase feature in the observation. The CTL experiment cannot reproduce the observed mixed-phase feature. A large portion of the clouds is a liquid phase with the liquid fraction close to 1 in CTL, which significantly overestimates the liquid fraction in the clouds. This is vastly different from previous versions of CAM. CAM5 showed an underestimation of the liquid fraction (Liu et al., 2011), while CAM3 showed a decrease of the liquid fraction with height due to its use of a temperature-dependent phase partitioning (Liu et al., 2007). Note that the modeled liquid fraction distributes on discrete vertical levels (Fig. 9b, c) due to a coarse model vertical resolution (with only 10 vertical levels below 2 km). In contrast, observed data were detected at 10 s^{-1} resolution during spiral ascents and descents in the clouds so that observed liquid fraction is distributed continuously with height.

The SIP_PHIL experiment better captures the mixed-phase feature in the bottom half of the clouds, with the liquid fraction varying between 0 to 1 (Fig. 9c). The increase of ice mass fraction in the lower portion of the clouds results from the ice growth by riming of cloud liquid and ice sedimentation from the upper levels. In the upper portion of the clouds, observed liquid fraction is larger than 0.6 with the mean value increases with height. The CTL experiment features “too much liquid and too little ice” in the mixed-phase clouds, while the SIP_PHIL experiment improves the model simulation of cloud phase with increased ice fraction at lower altitudes by adding an extra source of ice crystals from SIP.

https://doi.org/10.5194/acp-2020-1276
Preprint. Discussion started: 28 December 2020

For the cloud occurrence, 62.7% of observed clouds are mixed-phase, and only 16% are liquid-phase during the single-layer stratus period, as shown in Table 3. The liquid phase cloud occurrence is 73% in CTL and only 26.9% for mixed-phase clouds, indicating too much liquid-phase and too less mixed-phase occurrence in CAM6. The mixed-phase cloud occurrence is 58.8% in SIP_PHIL and agrees much better with the observation. Thus, there are more frequent mixed-phase clouds in SIP_PHIL, but the occurrence of ice clouds are still underestimated in SIP_PHIL. Note that, we define the modeled clouds with total cloud water amount larger than 0.001 g m^{-3} and the liquid fraction between 0.5% and 99.5% as the mixed-phase clouds, which are consistent with the observation (McFarquhar et al., 2007).

4.3 SIP impact on ice crystal number concentration

4.3.1 Vertical distribution of ice crystal number concentration

The vertical distribution of ICNCs in the single-layer boundary-layer mixed-phase stratus clouds on October 9, 10, and 11 from model simulation and observation is shown in Figure 10. Here, the ICNCs from the model only include ice particles with diameter larger than 53 μm to be consistent with the observed size limit for ice particles. In single-layer mixed-phase clouds, the measured ICNCs ranged from 0.1 to 100 L^{-1}, with an average value of 5 L^{-1}. The CTL experiment underestimates the ICNCs in all the cloud layers, with

https://doi.org/10.5194/acp-2020-1276
Preprint. Discussion started: 28 December 2020

Atmospheric Chemistry and Physics Discussions

a mean ICNC of ~0.25 L^{-1} and the maximum concentration of 3 L^{-1}. The mean ICNC is increased to ~1 L^{-1} in the SIP_PHIL experiment with a maximum concentration of 100 L^{-1}, which are in better agreement with the observations compared to CTL. ICNCs are increased by more than one order of magnitude in the lower portion of the clouds, although they are still lower than those observed in the upper portion of the clouds.

Fig. 10 also shows the linear regressions of ICNCs as a function of cloud altitude (black lines). The ICNC increases towards the cloud base in the observation, revealing ice multiplication during the ice growth and sedimentation. The CTL experiment shows that the ICNC decreases towards the cloud base, an opposite pattern compared to the observation. The observed pattern in the vertical profile of ICNCs is well captured in SIP_PHIL (Fig. 10c), suggesting that SIP is an important source of ice crystals near the cloud base in the Arctic boundary-layer mixed-phase stratus. Furthermore, the vertical distribution of ice particles is important for the longevity of the Arctic mixed-phase clouds, which features lower ICNCs in the upper portion of clouds and higher ICNCs towards the cloud base.

4.3.2 PDF of ice crystal number concentration

Figure 11 shows the probability density function (PDF) (i.e., the frequency of occurrence) of ICNCs from model simulations and observations for the boundary-layer mixed-phase stratus period (October 9-12, 2004). Note that only particles with a diameter

https://doi.org/10.5194/acp-2020-1276
Preprint. Discussion started: 28 December 2020

Atmospheric Chemistry and Physics Discussions

greater than 53 μm are included in the observed and modeled ICNCs. The PDF distribution in SIP_PHIL shows a shift to the right, with the ICNC peak much closer to the observations than CTL. The median ICNC is 0.26 L^{-1} in CTL, shifting to 0.48 L^{-1} in SIP_PHIL, which is closer to the observed median value of 1.27 L^{-1}.

The PDF distribution in SIP_PHIL also has a broader distribution than CTL. A broader distribution indicates that the maximum concentrations are higher in the observation and SIP_PHIL compared to CTL. In CTL experiment, the frequency of occurrence of ICNCs is much lower (higher) than observations when their values are higher (lower) than 0.5 L^{-1}. These biases in ICNCs PDF are much improved in SIP_PHIL, leading to a better agreement with the observation. The frequency occurrence of ICNC at 1 L^{-1} is 0.5%, 1.5%, 1.5% in CTL, SIP_PHIL, and observation, respectively. Thus, SIP_PHIL has an occurrence frequency of ICNC larger than 1 L^{-1}, which is 3 times of that in CTL.

4.3.3 Dependence of ice enhancement on cloud temperature

Figure 12 shows the bivariate joint PDF defined in terms of temperature and ice enhancement (N_{SIP_PHIL}/N_{CTL}) during the M-PACE. Strong ice enhancements are noticed at temperatures from –3 to –16°C, and ICNCs is increased by nearly 4 orders of magnitude in SIP_PHIL compared with CTL. As temperature decreases below –35°C, ice enhancement happens again, but with a reduced magnitude. For example, the largest enhancement at –44°C is around 3.2, with a frequency of 1% to 7%.

https://doi.org/10.5194/acp-2020-1276
Preprint. Discussion started: 28 December 2020

To investigate the dominant processes that contribute to the strong enhancement near –10 °C we plotted the bivariate joint PDF defined in terms of temperature and ice production rate (Fig. 13). A clear relationship between ice enhancement and fragmentation of freezing raindrops can be seen at temperatures from –20 to –4 °C in Figs. 12 and 13. The maximum ice production from the fragmentation of freezing raindrops is 160 L^{-1} ($10^{2.2}$) at temperatures ranging from 8 to –14 °C. Even though rime splintering also happens at temperatures between –8 to –3 °C with a maximum value of 20 L^{-1}, it is almost one order of magnitude lower than the fragmentation of freezing raindrops. Between –20 to –16 °C, primary ice nucleation and fragmentation of freezing raindrops coexist, with the fragmentation of freezing raindrops more efficient (with a magnitude of 10 L^{-1}) comparing to the primary ice nucleation (about 1 L^{-1}). Primary ice nucleation has the largest production of up to 250 L^{-1} at temperatures ranging from –32 to –25 °C. Below –35 °C, ice-ice collision break-up frequently happens, but with a lower process rate.

In summary, the strongest ice enhancement occurs in the moderately supercooled clouds with temperatures around –10°C. ICNC increases by up to 4 orders of magnitude mainly arising from the fragmentation of freezing rain. A weaker ice enhancement is noticed frequently in ice clouds with temperatures below –35°C, which is attributed to the ice-ice collision break-up.

https://doi.org/10.5194/acp-2020-1276
Preprint. Discussion started: 28 December 2020

Atmospheric Chemistry and Physics Discussions

5 Summary, conclusions and outlook

In this study, multiple SIP mechanisms are implemented in a GCM model (CAM6) to investigate their impacts on Arctic mixed-phase clouds, which were observed during the DOE ARM M-PACE field campaign. The CAM6 model with SIP provides a better simulation of the distinct "liquid cloud top, ice cloud base" feature of long-lived Arctic boundary-layer mixed-phase clouds.

We find that model biases of underestimation of mixed-phase cloud occurrence and overestimation of pure liquid cloud occurrence are reduced for the single-layer stratus after considering SIP. The mixed-phase cloud occurrence is 26.9%, 58.8%, and 62.7% in CTL, SIP_PHIL and the observation, respectively, while the pure liquid cloud occurrence is reduced from 73% in CTL to 40% in SIP_PHIL, in a better agreement with observed 16%.

We find that the pattern of the vertical distribution of ICNCs in the single-layer stratus is reversed after considering SIP in the model. The measured decrease of ICNC with cloud height is captured by SIP_PHIL but not by CTL. SIP also leads to a shift of PDF of ICNCs towards a more frequent occurrence of high ICNCs and less frequent occurrence of low ICNCs. We notice a taller PDF with higher peak and a broader tail in SIP_PHIL, indicating that high ICNCs occur more frequently with the occurrence of extreme high ICNCs ($>10^2$ L^{-1}) in SIP_PHIL, which is absent in CTL.

https://doi.org/10.5194/acp-2020-1276
Preprint. Discussion started: 28 December 2020

The maximum ICNC is around 3, 100, and 100 L^{-1} in CTL, SIP_PHIL, and observation, respectively, in the single-layer mixed-phase clouds. During the frontal cloud period, the SIP_PHIL experiment shows the largest absolute increases in IWC and ICNC by 6 mg m^{-3} and 7 L^{-1}, respectively. The largest ice enhancement (N_{SIP_PHIL}/N_{CTL}) is noticed during the transition period with a moderately cold cloud top temperature. The column integrated ICNC increases by five orders of magnitude and IWP increases by four orders of magnitude in SIP_PHIL compared to CTL. When comparing the relative importance between primary and secondary ice production, we notice that primary ice nucleation is more dominant in the deep clouds with cloud top reaching up to 10 km. At the same time, the fragmentation of freezing raindrops contributes more to ICNCs in the boundary-layer clouds.

The ice enhancement from SIP is strongest in moderately supercooled temperatures around –10 °C. ICNCs increase by up to 4 orders of magnitude. A weaker ice enhancement is noticed at ice clouds with temperatures below –35 °C, with a small, enhanced magnitude but unneglectable occurrence frequencies. At temperatures ranging from –4 to –20 °C, significant ice enhancement attributes to the fragmentation of freezing raindrops, with the maximum value of 160 at –10 °C. Primary ice nucleation has the largest production by up to 251 L^{-1} in the relatively cold-mixed phase clouds with temperatures between –32 to –25 °C.

https://doi.org/10.5194/acp-2020-1276
Preprint. Discussion started: 28 December 2020

Atmospheric Chemistry and Physics Discussions

In summary, the consideration of SIP in CAM6 results in a significant improvement in the model simulated mixed-phase clouds. It underscores the critical role of SIP in cloud microphysics, which should be considered in the parameterizations of GCMs.

Future work should also explore potential impacts of the graupel related SIP processes, and potential interactions of primary ice nucleation with SIP to impact cloud features. In this study, the parameterization of the HM process rate is based on Cotton et al. (1986), in this parameterization the ice production rate does not have a dependence on droplet size. However, it was found that this process rate also depends on the cloud droplet spectrum (Mossop, 1978; Phillips et al., 2001), in addition to temperature and the riming rate. Lacking the effect of cloud droplet spectrum in HM process is supposed to result in an overestimated splintering rate in the Arctic clouds, especially for the clouds which cloud-base is close to the freezing level and have small droplets in the cloud. For the ice fragmentation from ice-ice collisions, the graupel related collisions are not included, because the cloud microphysical scheme currently does not treat graupel. To quantify the impacts of graupel on SIP, the cloud microphysical scheme with prognostic graupel (Gettelman et al., 2019) or a “Single-Ice” microphysical scheme (Morrison and Milbrandt, 2015; Zhao et al., 2017) will be needed to further examine the impacts of graupel.

https://doi.org/10.5194/acp-2020-1276
Preprint. Discussion started: 28 December 2020

Competing interests: The authors declare that they have no conflict of interest.

Data availability: The model code is available at https://github.com/CESM-Development. The observation data of M-PACE campaign is obtained from the Atmospheric Radiation Measurement (ARM) user facility, a U.S. Department of Energy Office of Science, available at https://www.arm.gov/research/campaigns/nsa2004arcticcld.

Author contributions: XZ and XL conceptualized the analysis and wrote the manuscript with input from the co-authors. XZ modified the code, carried out the simulations, and performed the analysis. VP and SP provided the model code for the secondary ice production. VP and SP also provided scientific suggestions to the manuscript. XL was involved with obtaining the project grant and supervised the study. All authors were involved in helpful discussions and contributed to the manuscript.

Acknowledgment: This research was supported by the DOE Atmospheric System Research (ASR) Program (grant DE-SC0020510). We thank Meng Zhang for helpful discussions especially on processing the observation data.

https://doi.org/10.5194/acp-2020-1276
Preprint. Discussion started: 28 December 2020

Reference

Bennartz, R., Shupe, M. D., Turner, D. D., Walden, V. P., Steffen, K., Cox, C. J., Kulie, M. S., Miller, N. B., and Pettersen, C.: July 2012 Greenland melt extent enhanced by low-level liquid clouds, Nature, 496, 83-86, 10.1038/nature12002, 2013.

Cesana, G., and Chepfer, H.: Evaluation of the cloud thermodynamic phase in a climate model using CALIPSO-GOCCP, Journal of Geophysical Research Atmospheres, 118, 7922-7937, 10.1002/jgrd.50376, 2013.

Connolly, P. J., Heymsfield, A. J., and Choularton, T. W.: Modelling the influence of rimer surface temperature on the glaciation of intense thunderstorms: The rime–splinter mechanism of ice multiplication, Q J Roy Meteor Soc, 132, 3059-3077, 10.1256/qj.05.45, 2006.

Cotton, W. R., Tripoli, G. J., Rauber, R. M., and Mulvihill, E. A.: Numerical Simulation of the Effects of Varying Ice Crystal Nucleation Rates and Aggregation Processes on Orographic Snowfall, American Meteorological Society, 1658-1680, 1986.

Dearden, C., Vaughan, G., Tsai, T., and Chen, J. P.: Exploring the diabatic role of ice microphysical processes in two north atlantic summer cyclones, Mon Weather Rev, 144, 1249-1272, 10.1175/MWR-D-15-0253.1, 2016.

Field, P. R., Lawson, R. P., Brown, P. R. A., Lloyd, G., Westbrook, C., Moisseev, D., Miltenberger, A., Nenes, A., Blyth, A., Choularton, T., Connolly, P., Buehl, J., Crosier, J., Cui, Z., Dearden, C., DeMott, P., Flossmann, A., Heymsfield, A., Huang, Y., Kalesse, H., Kanji, Z. A., Korolev, A., Kirchgaessner, A., Lasher-Trapp, S., Leisner, T., McFarquhar, G., Phillips, V., Stith, J., and Sullivan, S.: Chapter 7. Secondary Ice Production - current state of the science and recommendations for the future, Meteorological Monographs, 58, 7.1-7.20, 10.1175/amsmonographs-d-16-0014.1, 2016.

Fu, S., Deng, X., Shupe, M. D., and Xue, H.: A modelling study of the continuous ice formation in an autumnal Arctic mixed-phase cloud case, Atmospheric Research, 228, 77-85, 10.1016/j.atmosres.2019.05.021, 2019.

Gettelman, A., and Morrison, H.: Advanced Two-Moment Bulk Microphysics for Global Models. Part I: Off-Line Tests and Comparison with Other Schemes, Journal of Climate, 28, 1268-1287, 2015.

Gettelman, A., Morrison, H., Thayer-Calder, K. and Zarzycki, C. M.: The Impact of Rimed Ice Hydrometeors on Global and Regional Climate, Journal of Advances in Modeling Earth Systems, 11(6), 1543–1562, doi:10.1029/2018MS001488, 2019.

Golaz, J.-C., Larson, V. E., and Cotton, W. R.: A PDF-Based Model for Boundary Layer Clouds. Part I: Method and Model Description, American Meteorological Society, 3540-3551, 2002.

Intrieri, J. M., Shupe, M. D., Uttal, T., and McCarty, B. J.: An annual cycle of Arctic cloud characteristics observed by radar and lidar at SHEBA, Journal of Geophysical Research: Oceans, 107, SHE 5-1, 10.1029/2000jc000423, 2002.

Jiang, H., Cotton, W. R., Pinto, J. O., Curry, J. A., and Weissbluth, M. J.: Cloud Resolving Simulations of Mixed-Phase Arctic Stratus Observed during BASE: Sensitivity to Concentration of Ice Crystals and Large-Scale Heat and Moisture Advection, American Meteorological Society, 2105-2117, 2000.

Kay, J. E., and Gettelman, A.: Cloud influence on and response to seasonal Arctic sea ice loss, Journal of Geophysical Research Atmospheres, 114, 10.1029/2009JD011773, 2009.

Larson, V. E., Golaz, J.-C., and Cotton, W. R.: Small-Scale and Mesoscale Variability in Cloudy Boundary Layers: Joint Probability Density Functions, Journal of the Atmospheric Sciences, 59, 3519-3539, 10.1175/1520-0469(2002)059<3519:SSAMVI>2.0.CO;2, 2002.

Korolev, A. and Field, P. R.: The Effect of Dynamics on Mixed-Phase Clouds: Theoretical Considerations, Journal of Atmospheric Sciences, 66–86, doi:https://doi.org/10.1175/2007JAS2355.1, 2008.

Liu, X., Easter, R. C., Ghan, S. J., Zaveri, R., Rasch, P., Shi, X., Lamarque, J. F., Gettelman, A., Morrison, H., Vitt, F., Conley, A., Park, S., Neale, R., Hannay, C., Ekman, A. M. L., Hess, P., Mahowald, N., Collins, W., Iacono, M. J., Bretherton, C. S., Flanner, M. G., and Mitchell, D.: Toward a minimal representation of aerosols in climate models:

https://doi.org/10.5194/acp-2020-1276
Preprint. Discussion started: 28 December 2020

description and evaluation in the Community Atmosphere Model CAM5, Geosci Model Dev, 5, 709-739, 2012.

Liu, X., Ma, P. L., Wang, H., Tilmes, S., Singh, B., Easter, R. C., Ghan, S. J., and Rasch, P. J.: Description and evaluation of a new four-mode version of the Modal Aerosol Module (MAM4) within version 5.3 of the Community Atmosphere Model, Geosci Model Dev, 9, 505-522, 2016.

Liu, X., and Penner, J. E.: Ice nucleation parameterization for global models, Meteorologische Zeitschrift, 499-514, 10.1127/0941-2948/2005/0059, 2005.

Liu, X., Xie, S., Boyle, J., Klein, S. A., Shi, X., Wang, Z., Lin, W., Ghan, S. J., Earle, M., Liu, P. S. K., and Zelenyuk, A.: Testing cloud microphysics parameterizations in NCAR CAM5 with ISDAC and M-PACE observations, Journal of Geophysical Research Atmospheres, 116, 10.1029/2011JD015889, 2011.

Liu, X., Xie, S., and Ghan, S. J.: Evaluation of a new mixed-phase cloud microphysics parameterization with CAM3 single-column model and M-PACE observations, Geophys Res Lett, 34, n/a-n/a, 10.1029/2007GL031446, 2007.

McFarquhar, G. M., Zhang, G., Poellot, M. R., Kok, G. L., McCoy, R., Tooman, T., Fridlind, A., and Heymsfield, A. J.: Ice properties of single-layer stratocumulus during the Mixed-Phase Arctic Cloud Experiment: 1. Observations, Journal of Geophysical Research Atmospheres, 112, 10.1029/2007JD008633, 2007.

Morrison, H., De Boer, G., Feingold, G., Harrington, J., Shupe, M. D., and Sulia, K.: Resilience of persistent Arctic mixed-phase clouds. Nature Publishing Group, 2012.

Morrison, H., and Milbrandt, J. A.: Parameterization of cloud microphysics based on the prediction of bulk ice particle properties. Part I: Scheme description and idealized tests, Journal of the Atmospheric Sciences, 72, 287-311, 10.1175/JAS-D-14-0065.1, 2015.

Mossop, S. C.: The influence of drop size distribution on the production of secondary ice particles during graupel growth, Q J Roy Meteor Soc, 104, 323-330, 10.1002/qj.49710444007, 1978.

Phillips, V. T. J., Blyth, A. M., Brown, P. R. A., Choularton, T. W., and Latham, J.: The glaciation of a cumulus cloud over New Mexico, Q J Roy Meteor Soc, 127, 1513-1534, 10.1002/qj.49712757503, 2001.

Phillips, V. T. J., Patade, S., Gutierrez, J., and Bansemer, A.: Secondary ice production by fragmentation of freezing drops: Formulation and theory, Journal of the Atmospheric Sciences, 75, 3031-3070, 10.1175/JAS-D-17-0190.1, 2018.

Phillips, V. T. J., Yano, J. I., and Khain, A.: Ice multiplication by breakup in ice-ice collisions. Part I: Theoretical formulation, Journal of the Atmospheric Sciences, 74, 1705-1719, 10.1175/JAS-D-16-0224.1, 2017a.

Phillips, V. T. J., Yano, J. I., Formenton, M., Ilotoviz, E., Kanawade, V., Kudzotsa, I., Sun, J., Bansemer, A., Detwiler, A. G., Khain, A., and Tessendorf, S. A.: Ice multiplication by breakup in ice-ice collisions. Part II: Numerical simulations, Journal of the Atmospheric Sciences, 74, 2789-2811, 10.1175/JAS-D-16-0223.1, 2017b.

Pinto, J. O.: Autumnal Mixed-Phase Cloudy Boundary Layers in the Arctic, American Meteorological Society, 2016-2038, 1998.

Schwarzenboeck, A., Shcherbakov, V., Lefevre, R., Gayet, J. F., Pointin, Y., and Duroure, C.: Indications for stellar-crystal fragmentation in Arctic clouds, Atmospheric Research, 92, 220-228, 10.1016/j.atmosres.2008.10.002, 2009.

Shupe, M. D., and Intrieri, J. M.: Cloud Radiative Forcing of the Arctic Surface: The Influence of Cloud Properties, Surface Albedo, and Solar Zenith Angle, American Meteorological Society, 616-628, 2004.

Shupe, M. D., Matrosov, S. Y., and Uttal, T.: Arctic mixed-phase cloud properties derived from surface-based sensors at SHEBA, Journal of the Atmospheric Sciences, 63, 697-711, 10.1175/JAS3659.1, 2006.

Sotiropoulou, G., Sullivan, S., Savre, J., Lloyd, G., Lachlan-Cope, T., Ekman, A. M. L., and Nenes, A.: The impact of secondary ice production on Arctic stratocumulus, Atmos Chem Phys, 20, 1301-1316, 10.5194/acp-20-1301-2020, 2020a.

Sotiropoulou, G., Vignon, E., Young, G., Morrison, H., O'Shea, S., Lachlan-Cope, T., Berne, A., and Nenes, A.: Secondary ice production in summer clouds over the

https://doi.org/10.5194/acp-2020-1276
Preprint. Discussion started: 28 December 2020

Atmospheric Chemistry and Physics
Discussions

Antarctic coast: an underappreciated process in atmospheric models, Atmos Chem Phys, 1-30, 10.5194/acp-2020-328, 2020b.

Sullivan, S. C., Hoose, C. and Nenes, A.: Investigating the contribution of secondary ice production to in-cloud ice crystal numbers, Journal of Geophysical Research: Atmospheres, 122(17), 9391–9412, doi:10.1002/2017JD026546, 2017.

Sullivan, S. C., Hoose, C., Kiselev, A., Leisner, T. and Nenes, A.: Initiation of secondary ice production in clouds, Atmospheric Chemistry and Physics, 18(3), 1593–1610, doi:10.5194/acp-18-1593-2018, 2018a.

Sullivan, S. C., Barthlott, C., Crosier, J., Zhukov, I., Nenes, A. and Hoose, C.: The effect of secondary ice production parameterization on the simulation of a cold frontal rainband, Atmospheric Chemistry and Physics, 18(22), 16461–16480, doi:10.5194/acp-18-16461-2018, 2018b.

Turner, D. D., Clough, S. A., Liljegren, J. C., Clothiaux, E. E., Cady-Pereira, K. E., and Gaustad, K. L.: Retrieving liquid water path and precipitable water vapor from the atmospheric radiation measurement (ARM) microwave radiometers, 3680-3689,

Verlinde, J., Harrington, J. Y., McFarquhar, G. M., Yannuzzi, V. T., Avramov, A., Greenberg, S., Johnson, N., Zhang, G., Poellot, M. R., Mather, J. H., Turner, D. D., Eloranta, E. W., Zak, B. D., Prenni, A. J., Daniel, J. S., Kok, G. L., Tobin, D. C., Holz, R., Sassen, K., Spangenberg, D., Minnis, P., Tooman, T. P., Ivey, M. D., Richardson, S. J., Bahrmann, C. P., Shupe, M., DeMott, P. J., Heymsfield, A. J., and Schofield, R.: The mixed-phase arctic cloud experiment, B Am Meteorol Soc, 88, 205-221, 10.1175/BAMS-88-2-205, 2007.

Wang, Y., Liu, X., Hoose, C., and Wang, B.: Different contact angle distributions for heterogeneous ice nucleation in the Community Atmospheric Model version 5, Atmos Chem Phys, 14, 10411-10430, 2014.

Wang, Z.: A refined two-channel microwave radiometer liquid water path retrieval for cold regions by using multiple-sensor measurements, Ieee Geosci Remote S, 4, 591-595, 10.1109/LGRS.2007.900752, 2007.

Xie, S., Boyle, J., Klein, S. A., Liu, X., and Ghan, S.: Simulations of Arctic mixed-phase clouds in forecasts with CAM3 and AM2 for M-PACE, Journal of Geophysical Research, 113, D04211-D04211, 10.1029/2007JD009225, 2008.

https://doi.org/10.5194/acp-2020-1276
Preprint. Discussion started: 28 December 2020

Atmospheric Chemistry and Physics Discussions

Xie, S., Klein, S. A., Yio, J. J., Beljaars, A. C. M., Long, C. N., and Zhang, M.: An assessment of ECMWF analyses and model forecasts over the North Slope of Alaska using observations from the ARM Mixed-Phase Arctic Cloud Experiment, Journal of Geophysical Research, 111, D05107-D05107, 10.1029/2005JD006509, 2006.

Xie, S., McCoy, R. B., Klein, S. A., Cederwall, R. T., Wiscombe, W. J., Clothiaux, E. E., Gaustad, K. L., Golaz, J. C., Hall, S. D., Jensen, M. P., Johnson, K. L., Lin, Y., Long, C. N., Mather, J. H., McCord, R. A., McFarlane, S. A., Palanisamy, G., Shi, Y., and Turner, D. D.: ARM climate modeling best estimate data: A new data product for climate studies, B Am Meteorol Soc, 91, 13-20, 10.1175/2009BAMS2891.1, 2010.

Zhang, M., Liu, X., Diao, M., D'Alessandro, J. J., Wang, Y., Wu, C., Zhang, D., Wang, Z., and Xie, S.: Impacts of Representing Heterogeneous Distribution of Cloud Liquid and Ice on Phase Partitioning of Arctic Mixed-Phase Clouds with NCAR CAM5, Journal of Geophysical Research: Atmospheres, 124, 13071-13090, 10.1029/2019JD030502, 2019.

Zhang, M., Xie, S., Liu, X., Lin, W., Zhang, K., Ma, H. Y., Zheng, X., and Zhang, Y.: Toward Understanding the Simulated Phase Partitioning of Arctic Single-Layer Mixed-Phase Clouds in E3SM, Earth and Space Science, 10.1029/2020ea001125, 2020.

Zhao, X., Lin, Y., Peng, Y., Wang, B., Morrison, H., and Gettelman, A.: A single ice approach using varying ice particle properties in global climate model microphysics, Journal of Advances in Modeling Earth Systems, 9, 2138-2157, 10.1002/2017MS000952, 2017.

https://doi.org/10.5194/acp-2020-1276
Preprint. Discussion started: 28 December 2020

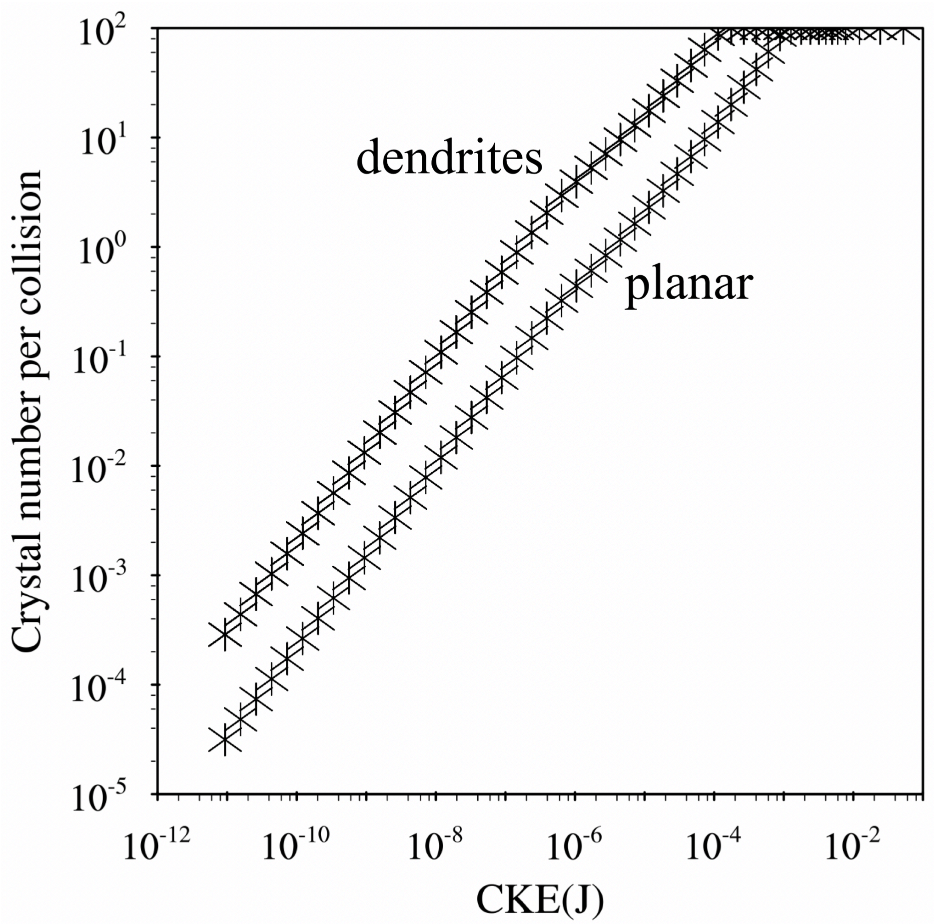

Figure 1. The number of fragments per collision as a function of initial kinetic energy (CKE).

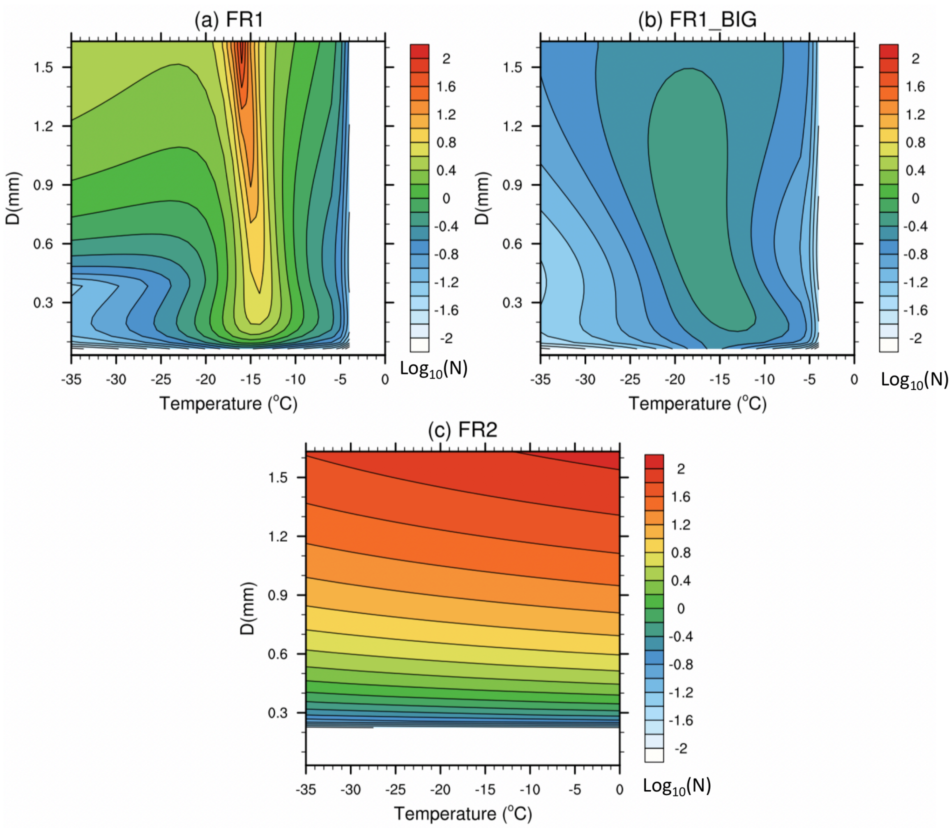

Figure 2. The number of fragments per frozen drop (shown as $\log_{10}$N) as a function of temperature and particle diameter, from (a) mode 1 of the rain freezing fragmentation (FR1), (b) mode 1 of the rain freezing fragmentation but for the big fragments (FR1_BIG), and (c) mode 2 of the rain freezing fragmentation (FR2).

https://doi.org/10.5194/acp-2020-1276
Preprint. Discussion started: 28 December 2020

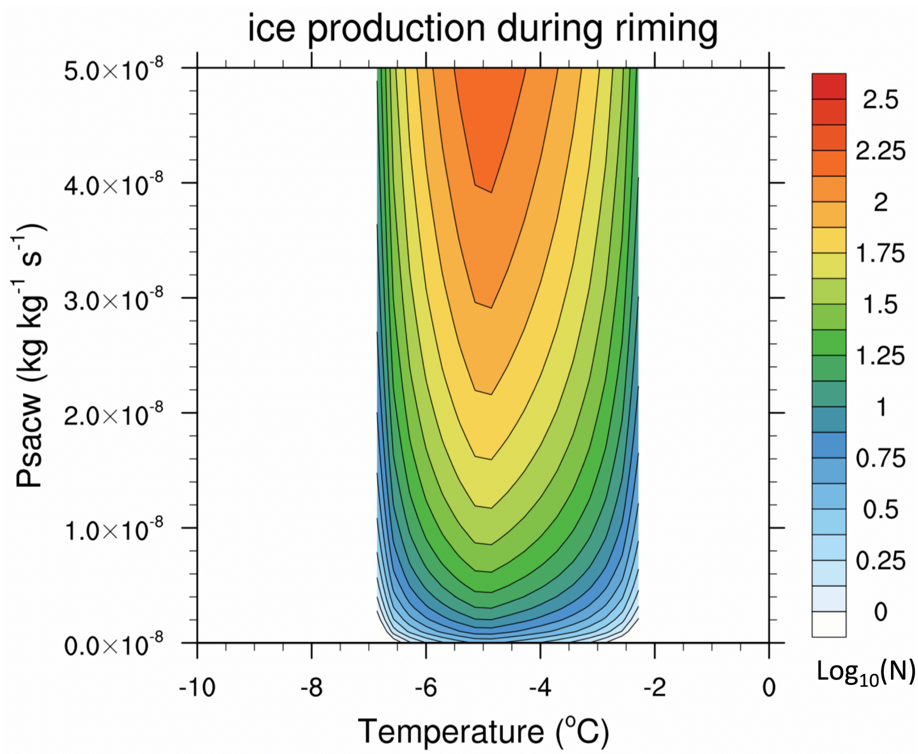

763

764 Figure 3. The rime splintering rate (shown as $\log_{10}N$) as a function of temperature and

765 riming rate.

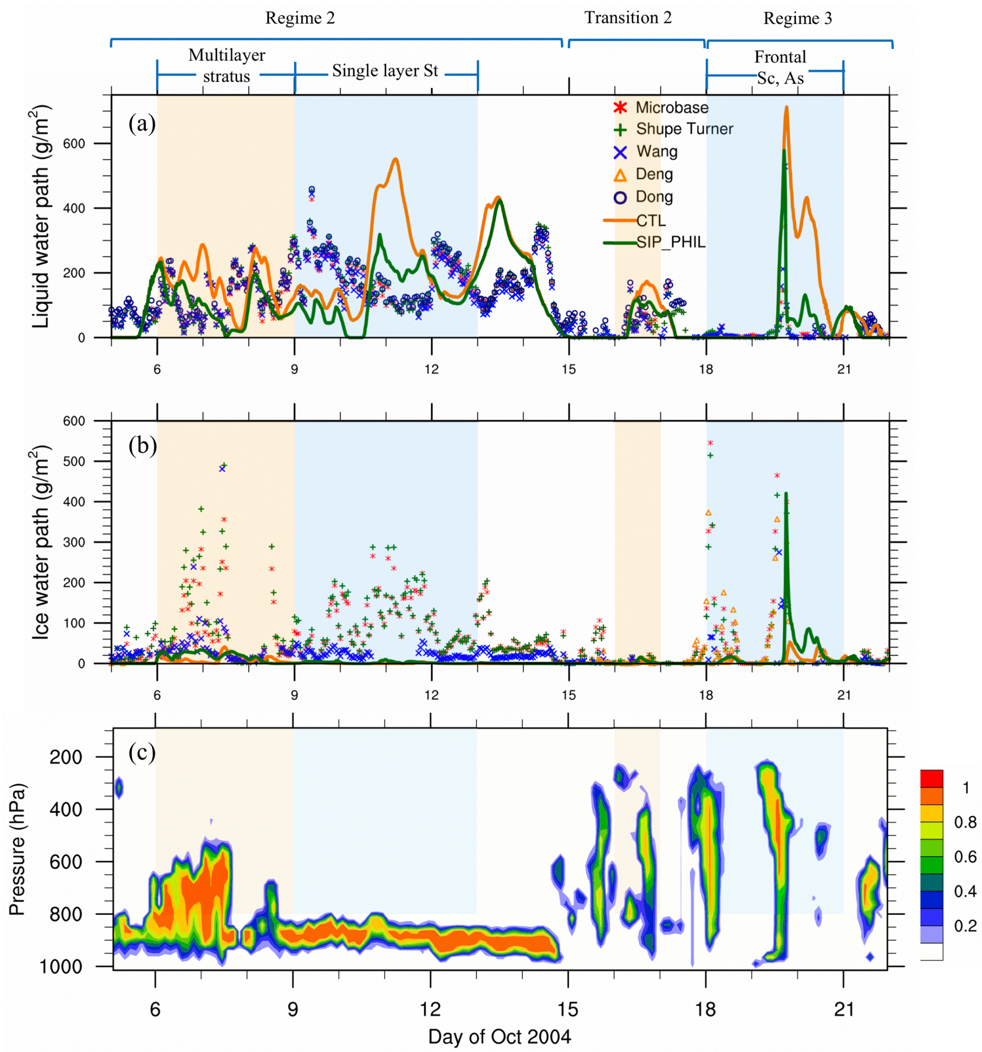

Figure 4. Temporal evolution of (a) LWP, (b) IWP from remote sensing retrievals shown as different markers, CTL experiment (orange solid line) and SIP_PHIL experiment (dark green solid line), and (c) observed time-pressure cross section of the cloud fraction. The shadings show the multilayer stratus, single-layer stratus, transition, and frontal periods.

772 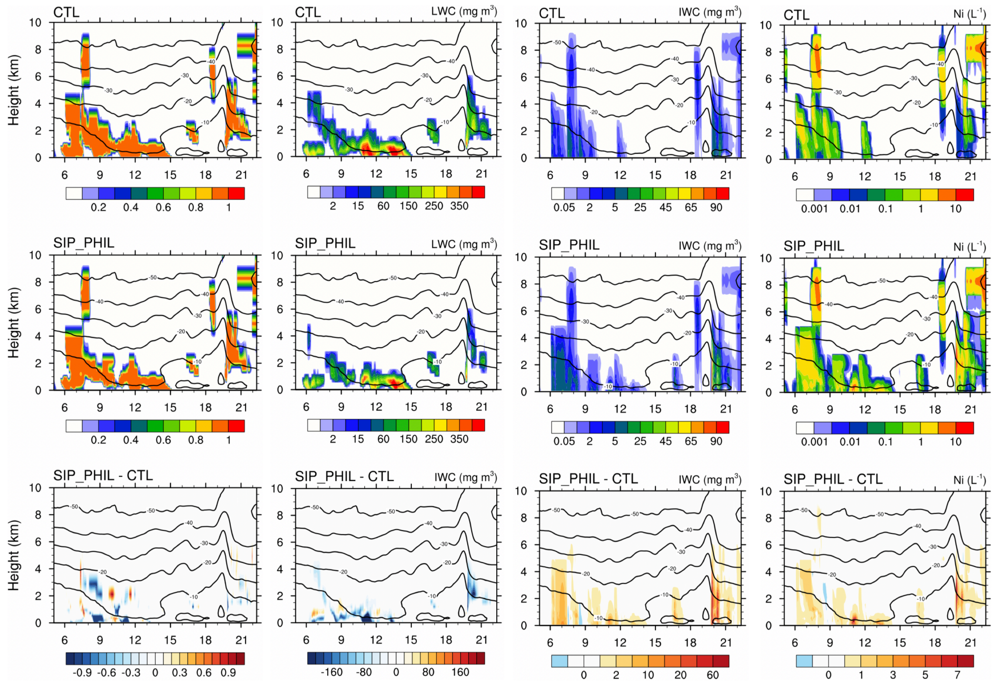

773 Figure 5. Time-height cross section of cloud fraction (first column), LWC (second
774 column), IWC (third column) and ice crystal number concentration (fourth column) from
775 CTL (first row), SIP_PHIL (second row) and the differences between SIP_PHIL and
776 CTL (SIP_PHIL minus CTL, third row).

777

https://doi.org/10.5194/acp-2020-1276
Preprint. Discussion started: 28 December 2020

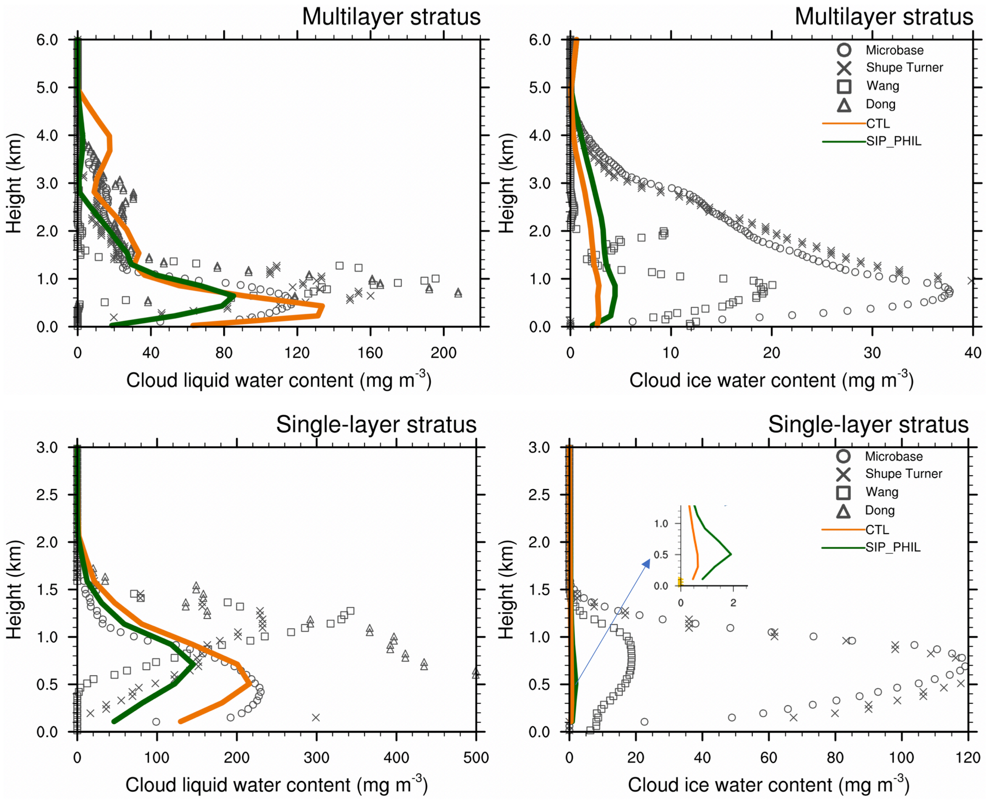

Figure 6. Vertical profiles of IWC and LWC during multilayer stratus and single-layer stratus periods from remote sensing retrievals shown as different markers, CTL experiment (orange solid line) and SIP_PHIL experiment (dark green solid line).

https://doi.org/10.5194/acp-2020-1276
Preprint. Discussion started: 28 December 2020

Atmospheric Chemistry and Physics Discussions

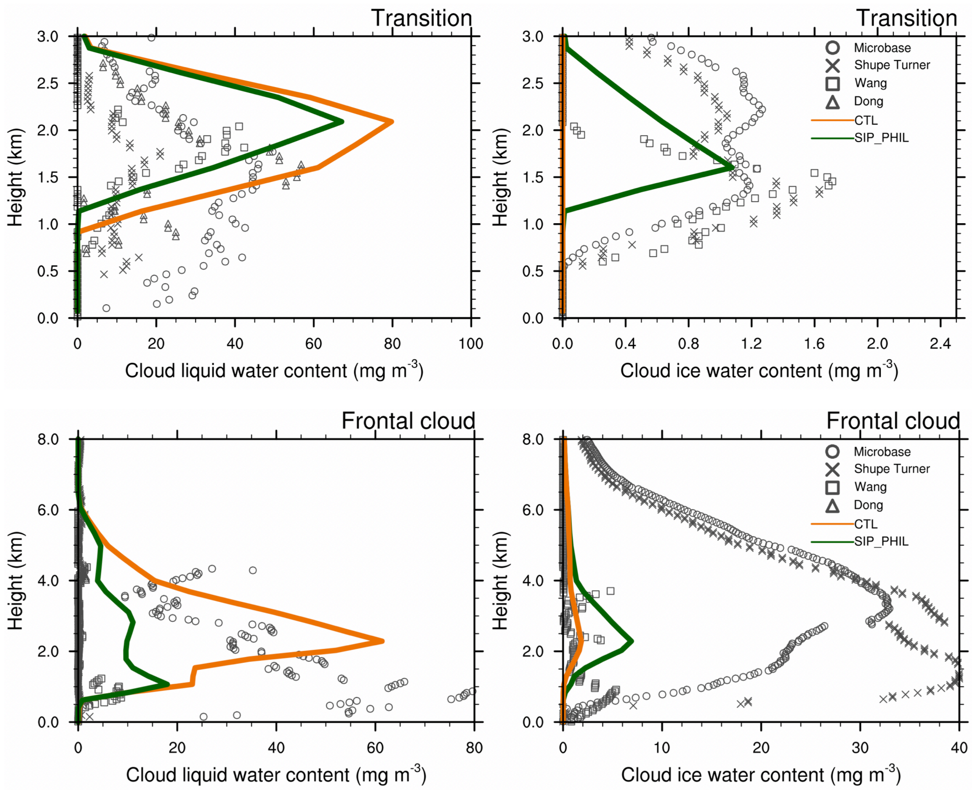

Figure 7. Vertical profiles of IWC and LWC during the transition and frontal cloud periods, from remote sensing retrievals shown as different markers, CTL experiment (orange solid line) and SIP_PHIL experiment (dark green solid line).

https://doi.org/10.5194/acp-2020-1276
Preprint. Discussion started: 28 December 2020

Atmospheric Chemistry and Physics Discussions
Open Access

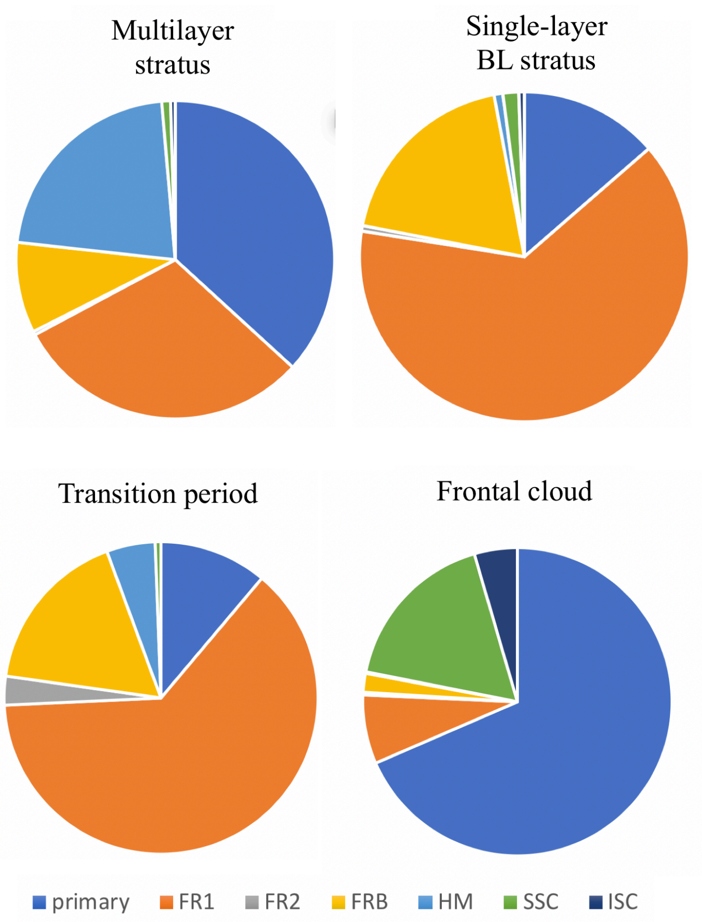

Figure 8. Pie charts showing the relative contributions to total ice production from primary production (i.e., ice nucleation), rime splintering (HM), fragmentation of frozen rain (including the small fragments in the first mode (FR1), big fragments in the first mode (FRB), and the second mode (FR2)), breakup from ice–ice collisions (including snow and cloud ice collision (ISC) and snow and snow collision (SSC)) during the four M-PACE periods, the vertically integrated process rates are used in the plot.

https://doi.org/10.5194/acp-2020-1276
Preprint. Discussion started: 28 December 2020

Atmospheric Chemistry and Physics Discussions

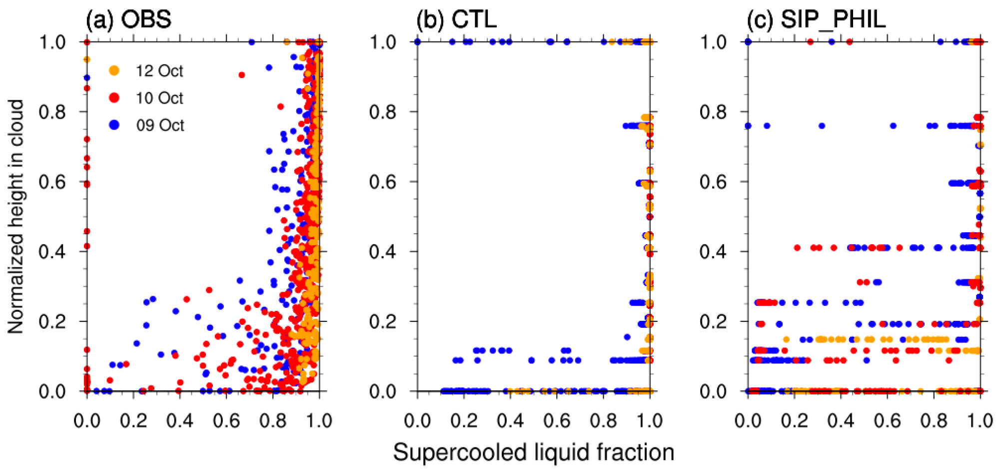

Figure 9. Liquid fraction as a function of normalized cloud height from cloud base. The normalized cloud altitude Z_n is defined as: $Z_n = \frac{z - Z_b}{Z_t - Z_b}$, in which z is the altitude, Z_b is the altitude of cloud base, and Z_t is the altitude of cloud top, from (a) observation, (b) CTL, and (c) SIP_PHIL.

https://doi.org/10.5194/acp-2020-1276
Preprint. Discussion started: 28 December 2020

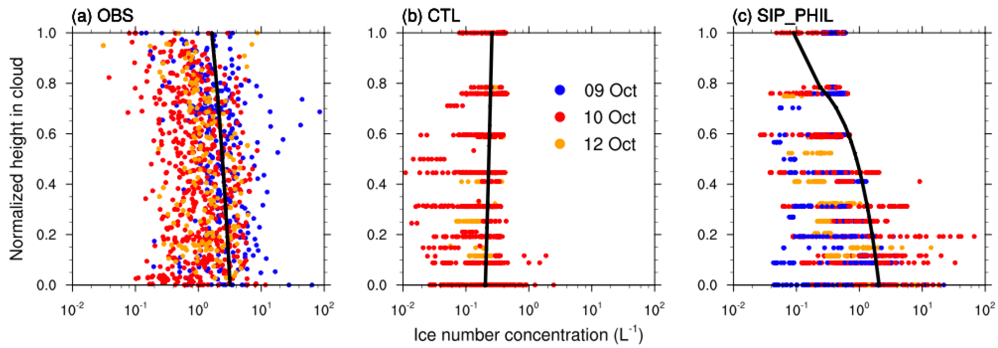

Figure 10. Ice number concentration as function of normalized cloud height from cloud base, black solid lines show the linear regression line between ice number concentration and height, from (a) observation, (b) CTL, and (c) SIP_PHIL.

https://doi.org/10.5194/acp-2020-1276
Preprint. Discussion started: 28 December 2020

Atmospheric Chemistry and Physics Discussions

814 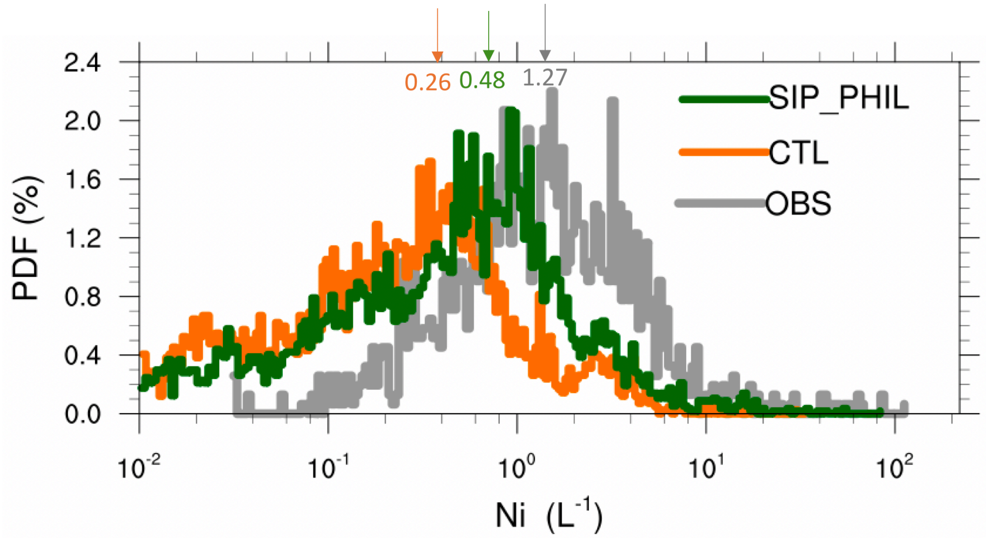

815 Figure 11. The probability density function (PDF) of ice crystal number concentrations
816 from observation (gray line), CTL (orange line), and SIP_PHIL simulations (green line).
817 The arrow indicates the median of each distribution which means that the set of values
818 less (or greater) than the median has a probability of 50%.
819
820
821

https://doi.org/10.5194/acp-2020-1276
Preprint. Discussion started: 28 December 2020

Atmospheric Chemistry and Physics
Discussions

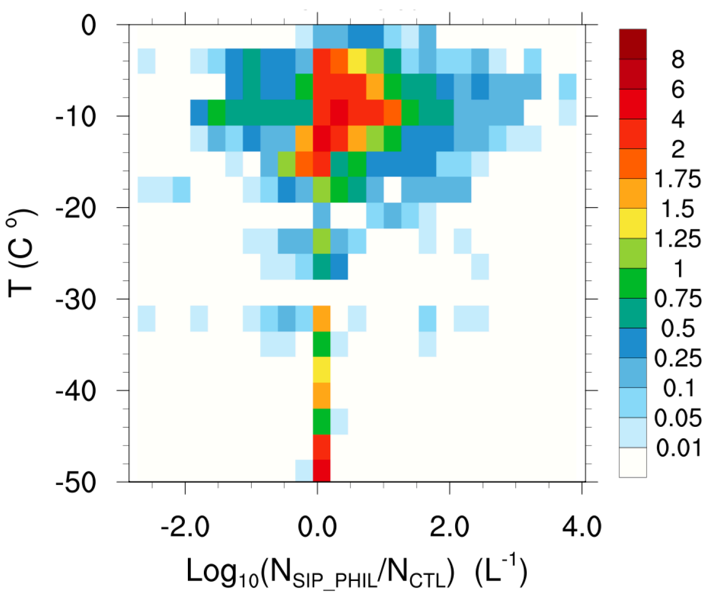

Figure 12. Bivariate joint probability density function of ice enhancement defined in terms of both temperature and ice enhancement. The ice enhancement is defined as $\mathrm{Log}_{10}(N_{SIP\_PHIL} / N_{CTL})$.

https://doi.org/10.5194/acp-2020-1276
Preprint. Discussion started: 28 December 2020

Atmospheric Chemistry and Physics Discussions

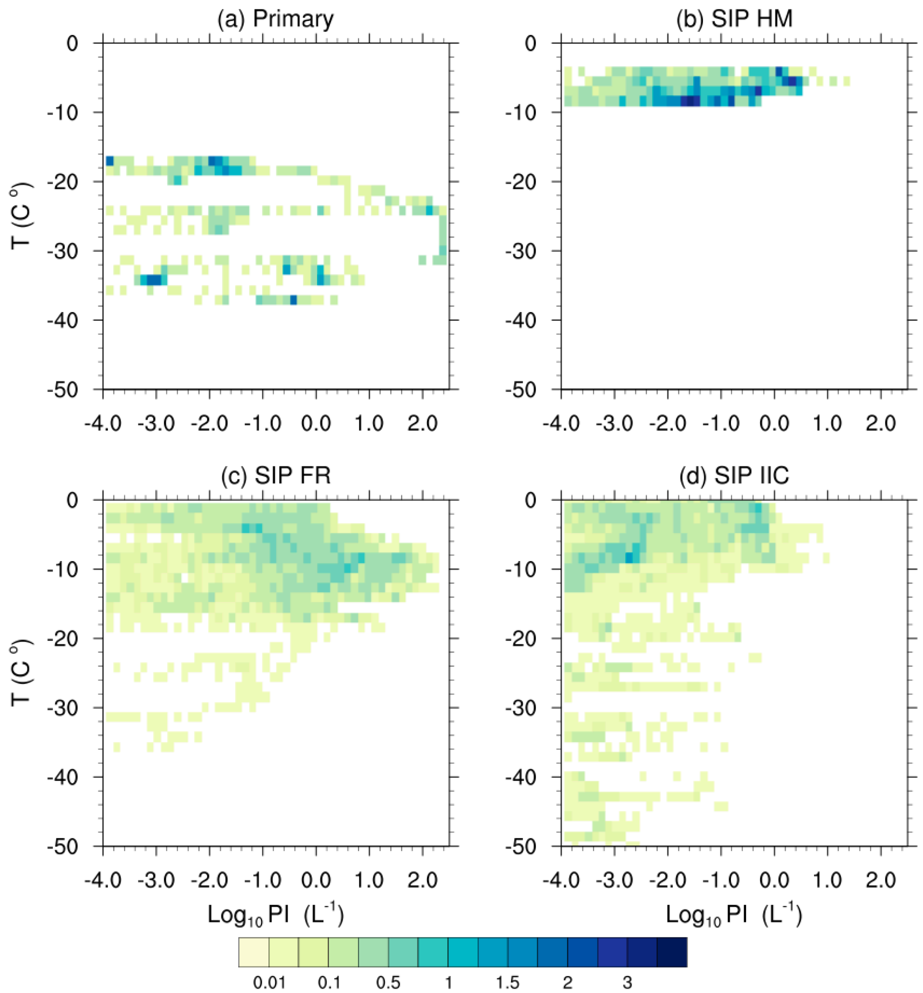

Figure 13. Bivariate joint probability density function of ice production defined in terms of temperature and ice production, (a) primary ice production; (b) ice production from riming splintering; (c) ice production from rain fragmentation; (d) ice production from ice-ice collision. The ice production (PI, with unit of :# L^{-1}) is calculated as ice production rate ($L^{-1}s^{-1}$) multiplied by model time step (20 mins), shown in Log_{10}.

https://doi.org/10.5194/acp-2020-1276
Preprint. Discussion started: 28 December 2020

Atmospheric Chemistry and Physics Discussions
Open Access

Table 1. List of experiments.

	Type of Secondary ice production	References
CTL	Riming splintering	[Cotton et al., 1986]
SIP_PHIL	Riming splintering	[Cotton et al., 1986]
	Ice-ice collision fragmentation	[Phillips et al., 2017]
	Rain freezing fragmentation	[Phillips et al., 2018]
CTL_no_HM	Same as CTL, but no HM process	

https://doi.org/10.5194/acp-2020-1276
Preprint. Discussion started: 28 December 2020

Table 2. The temporally-averaged IWP, LWP (unit: g m^{-2}), and vertically-integrated ice crystal number concentration (unit: m^{-2}) during the four periods from observation, and CTL and SIP_PHIL experiments.

		Multilayer stratus	Single-layer stratus	Transition	Frontal cloud
	OBS	55.6	74.7	5.6	97.0
IWP	CTL	11.2	0.9	0.0001	10.4
	SIP_PHIL	17.1	2.5	3.6	26.1
	OBS	134.4	190.2	58.3	50.2
LWP	CTL	165.1	217.6	88.4	127.6
	SIP_PHIL	102.8	131.0	62.1	41.2
ICNC	CTL	5.77×10^{6}	3.22×10^{5}	7.66	2.26×10^{6}
	SIP_PHIL	7.09×10^{6}	1.3×10^{6}	4.57×10^{5}	4.67×10^{6}

Table 3. Percentage of occurrence of liquid, mixed-phase, and ice clouds during single layer mixed-phase clouds from observation, and CTL and SIP_PHIL experiments.

	Liquid	Mixed-phase	Ice
OBS (%)	16	62.7	22.3
CTL (%)	73	26.9	0.1
SIP_PHIL (%)	40	58.8	1.2